Supporting Information

Two Hydrated Ionic Cocrystals of Phenylphosphonate Exhibiting Second-Harmonic Generation and Proton Conductivity

Peng Zhuang, [abc] *Chun-Li Hu,* [a] *Bing-Ping Yang*,* [abc] *and Jiang-Gao Mao* [abc]

[a] State Key Laboratory of Functional Crystals and Devices, Fujian Institute of Research on the Structure of Matter, Chinese Academy of Sciences, Fuzhou, 350002, P.R. China

[b] University of Chinese Academy of Sciences, Beijing, 100049, P.R. China

[c] Fujian College, University of Chinese Academy of Sciences, Fuzhou, 350002, P.R. China

E-mail: ybp@fjirsm.ac.cn

Table of contents

Experimental Section

Synthesis of $[C(NH_2)_3]_2(PhPO_3)\cdot 2H_2O$ (1): Phenylphosphonic acid (2.5 mmol) and guanidine carbonate (5.0 mmol) were added to a 25 mL beaker containing 10 mL of deionized water. The mixture was stirred at 75 °C for 20 minutes until a clear solution formed. Then, the beaker was placed in a fume hood for slow evaporation at room temperature. Colorless block crystals were formed after approximately seven days. The yield was about 87.21%.

Synthesis of $(C_5H_7N_2)_2(PhPO_3)\cdot 5H_2O$ (2): Phenylphosphonic acid (2 mmol) and 4-aminopyridine (4 mmol) were added to 15 mL of deionized water in a 25 mL beaker. The mixture was stirred at 75 °C for 20 minutes to produce a clear solution. After slow evaporation of the solution in a fume hood for approximately one week, colorless block crystals were obtained. The yield was 30.25%.

Crystal Growth: The crystal growth experiment was conducted using the seeded solution growth method (Figure S17). First, A crack-free, optically transparent seed crystal was immersed in a solution prepared with stoichiometric ratios of the reactants. Then, the solvent was slowly evaporated. Centimeter-sized single crystals were obtained over the course of one month.

Single-Crystal X-ray Diffraction Analysis: Single crystals of comounds **1** and **2** were selected and ground to the appropriate dimensions. A high-quality crystal of each compound was mounted on a loop first and subsequently mounted on a goniometer for data collection. The diffraction data for **1** were collected using Mo Kα radiation (λ = 0.71073 Å) at a temperature of 150.15 K on a Rigaku Oxford Diffraction SuperNova CCD diffractometer. The data for compound **2** were collected using Cu Kα radiation (λ = 1.54184 Å) at a temperature of 293 K using the same instrument. Cell refinement and data reduction were performed using the CrysAlisPro software. Numerical absorption correction based on Gaussian integration over a multifaceted crystal model and empirical absorption correction using spherical harmonics were implemented in the SCALE3 ABSPACK scaling algorithm.[1] The structures were solved by direct methods and refined by full-matrix least-squares on F^2 using SHELXL.[2,3] All non-hydrogen atoms were refined anisotropically. The structures were checked for higher symmetry using PLATON, and no additional symmetry was found.[4] The Flack parameters were refined to 0.11(5) for **1** and 0.009(13) for **2**, thereby confirming the correct absolute structures.[5] Relevant crystallographic data are summarized in the Supporting Information (Tables S2–S5).

Powder X-ray Diffraction: PXRD data were collected on a Rigaku MiniFlex600 diffractometer equipped with a graphite monochromator and utilizing Cu Kα radiation (λ = 1.54186 Å). The data were acquired over the 2θ range of 5–70° with a step size of 0.02°.

Spectroscopic Measurements: Fourier-transform infrared (FTIR) spectra were obtained using a Bruker Vertex 70 FT-IR spectrometer. The spectra ranged from 4000 to 400 cm^{-1}, with a resolution of 2 cm^{-1}, at room temperature. The attenuated total reflection (ATR) technique was employed to acquire the spectra. The UV-vis-NIR diffuse reflectance spectra were measured in the 200–2000 nm range using a PerkinElmer Lambda 950 spectrophotometer, with $BaSO_4$

powder serving as a 100% reflectance reference. The absorption data were derived from the diffuse reflectance data using the Kubelka-Munk function:

$F(R) = (1 - R)^2/(2R) = K/S\#Equation(1)$

where K is the absorption coefficient and S is the scattering coefficient.[6] The band gap was determined by extrapolating the absorption edge to the baseline on the plot of $F(R)$ versus energy.

Thermal Analyses: Thermogravimetric analysis was performed in conjunction with differential thermal analysis, using a NETZSCH STA 499C apparatus. Approximately 3.0–6.0 mg of powder were placed in an alumina crucible and heated from 25 to 800°C at a rate of 15 °C min^{-1} under a continuous nitrogen flow.

SHG Measurements: The powder SHG of the compounds was measured using a method based on that of Kurtz and Perry.[7] A Q-switched Nd:YAG laser emitting 1064 nm radiation was used as the light source. The pure polycrystalline samples were ground and sieved into six distinct particle size ranges (25–45, 45–53, 53–75, 75–109, 109–150, and 150–210 μm). Samples of KDP with equivalent particle size ranges were used as references. The SHG signals for **1**, **2**, and KDP within the 150–210 μm particle size range were recorded on an oscilloscope.

LDT Measurements: The LDT for crystalline samples of **1** and **2** were measured using a Q-switched pulsed laser (1064 nm, 10 ns, 1 Hz). In this procedure, a single site on the crystal was irradiated with a laser pulse. The pulse energy was then increased incrementally until damage occurred. The LDT was calculated using the following equation:

$I = E/(\tau \times A)\#Equation(2)$

where I is the LDT value, E is the input energy at the damage point, τ is the laser pulse width, and A is the area of the circular laser spot.

Birefringence Measurements: The birefringences of crystals were measured with a polarizing light microscope (ZEISS Axio Scope A1), by means of tilting the compensator and compensating the optical path difference. The birefringence was calculated according to the following equation:

$\Gamma = \Delta n \times T\#Equation(3)$

where Γ denotes the optical path difference, Δn represents the birefringence, and T is the thickness of the crystal.

Computational Methods: The calculations of the electronic and optical properties were performed with the CASTEP code using the plane-wave pseudopotential DFT.[8,9] The generalized gradient approximation (GGA) Perdew-Burke-Ernzerhof (PBE) was chosen as the exchange correlation functional.[10] The core electron interactions were represented by the norm-conserving pseudopotential.[11] H $1s^1$, C $2s^25p^2$, N $2s^25p^3$, O $2s^22p^4$, and P $3s^23p^3$ orbital electrons were set as the valence electrons. A cutoff energy of 750 eV was used to determine of the number of plane-wave basis sets. The Monkhorst-Pack k-point samplings for numerical integration over the Brillouin zone were 2 × 3 × 2 and 4 × 1 × 3 for compound **1** and **2**, respectively. More than 472 and 332 empty bands were used in the optical property calculations

for compound **1** and **2**, respectively. The calculations of the second-order NLO susceptibilities were based on the length gauge formalism within the independent particle approximation.[12,13] The second-order NLO susceptibility can be expressed as:

$$\chi_{L}^{abc}(-2\omega;\omega,\omega) = \chi_{inter}^{abc}(-2\omega;\omega,\omega) + \chi_{intra}^{abc}(-2\omega;\omega,\omega) + \chi_{mod}^{abc}(-2\omega;\omega,\omega) \#Equation(4)$$

where the subscript L denotes the length gauge, χ_{inter}^{abc} , χ_{intra}^{abc} and χ_{mod}^{abc} give the contributions to χ_{L}^{abc} from interband processes, intraband processes, and the modulation of interband terms by intraband terms, respectively. To gain further understanding of the anion groups, the electronic structures of the $[C(NH_2)_3]^+$ and $(C_5H_7N_2)^+$ groups were calculated at the molecular level using the Gaussian09 package. The calculations were performed using the B3LYP functional with the 6-31G basis set, a computational setting widely validated and employed in quantum chemical calculations. The electrostatic potential (ESP) was calculated using the DMol3 software package with the GGA-BLYP functional.

Proton conductivity: The powder samples were pressed into discs using a steel mold. These discs were subsequently assembled with stainless steel sheets to form a sandwich structure. The electrolyte solution was composed of 5 mM $K_4Fe(CN)_6$ and 0.1 M KCl. Electrochemical impedance spectroscopy measurements were conducted at room temperature. The proton conductivity (σ) was calculated using the following equation:

$$\sigma = L/(S \times R) \#Equation(5)$$

where L (cm) is the thickness of the sample, S (cm²) is the contact area, and R (Ω) is the bulk resistance. The bulk resistance was obtained by direct calculation from the intercept of the semicircle in the high-frequency region of the Nyquist plot.

Table S1. Phosphate nonlinear optical crystals reported in the past three years.

Compound	S.G.	SHG	Δn_{exp}	Δn_{cal}	Eg_{exp}	Ref
$Ag(Te_2O_3)(PO_4)$	$Pmn2_1$	2.1	0.045@546	0.037@546	3.98	[14]
$PbBi_3PO_8$	$I4mm$	2.3	-	-	3.14	[15]
$KMg[B(PO_4)_2](H_2O)_2$	$P6_122$	0.13	-	-	4.61	[16]
$NaMg(H_2O)_2(BP_2O_8)(H_2O)$	$P6_122$	0.10	-	-	4.54	[16]
$LiMg(H_2O)_2(BP_2O_8)(H_2O)$	$P6_122$	0.17	-	-	4.65	[16]
$Li_2Rb_2P_2O_7$	$Pca2_1$	0.2	-	-	4.98	[17]
$LiK_2RbP_2O_7$	$C222_1$	0.2	-	-	4.33	[17]
$Al_2(PO_4)_2(H_2O)_4$	$P2_12_12_1$	0.68	-	-	3.89	[18]
$LiBePO_4$	Cc	1.3	0.018@590	0.016@590	-	[19]
BeP_2O_6	$P2_1$	2.1	0.028@590	0.024@590	-	[19]
$(NH_4)_3[Sc_3F_5(PO_4)](PO_3F)_2$	Cc	0.65	0.01@550	0.008@550	6.2	[20]
$LiNH_4B_2P_2O_9$	$P2_12_12_1$	0.4	0.005@546	0.006@1064	-	[21]
$LiKB_2P_2O_9$	$P2_12_12_1$	0.9	0.006@546	0.006@1064	-	[21]
$Li_3[AlP_2O_7F(OH)](H_2O)_{0.5}$	$P4$	0.17	-	-	3.6	[22]
$K[Al_2(PO_4)_2F(H_2O)]$	$P2_12_12_1$	0.11	-	-	4.24	[22]
$MgPO_2F_3$	$Imm2$	0.92	-	0.046@1064	-	[23]
Mg_2PO_4Cl	$Pna2_1$	5.2	-	0.046@1064	-	[24]
$Pb_6(HPO_3)_2Br_8(H_2O)\cdot H_2O$	$P1$	1.02	-	0.040@1064	3.61	[25]
$GeHPO_3$	$Pna2_1$	10.3	0.062@546	0.053@546	-	[26]
$Sc(H_2PO_3)_3$	$P2_12_12_1$	0.6	-	0.033@1064	4.05	[27]
$NaPO_3NH_3$	$P6_3$	1.2	0.062@546	0.062@546	6.5	[28]
$RbZnPO_4$	$P2_1$	1.2	-	0.008@1064	5.49	[29]
$CsZnPO_4$	$Imm2$	0.5	-	-	5.37	[29]
BeH_3PO_5	$Pna2_1$	0.7	-	0.066@400	-	[30]
$Li_2RbBi(PO_4)_2$	$P2_1$	5.2	-	0.035@1064	-	[31]
$(NH_4)_3(H_3O)Zn_4(PO_4)_4$	$P6_3$	1.4	-	0.032@1064	3.69	[32]
$Cs_3[(BOP)_2(B_3O_7)_3]$	$R3$	3	0.077@1064	0.075@532	-	[33]
$LiZnPO_4$	Cc	2.3	-	0.005@1064	4.9	[34]
$KZnPO_4$	$P6_3$	0.2	-	0.011@1064	4.87	[34]
$K_2Na_3B_2P_3O_{13}$	$Cmc2_1$	0.42	-	0.011@1064	-	[35]
$(C_2N_4OH_7)H_2PO_3$	Cc	2.2	0.19@589.3	0.195@532	-	[36]
$C(NH_2)_3H_2PO_3$	$P2_1$	1.4	-	0.089@532	-	[36]
$[C(NH_2)_3]_2[CH_3PO_3]$	Cm	1	0.053@1064	0.053@1064	5.93	[37]
$R\text{-}(C_5H_{14}N_2)(HPO_4)\cdot H_2O$	$P2_1$	0.5	0.005@546	0.011@546	-	[38]
$S\text{-}(C_5H_{14}N_2)(HPO_4)\cdot H_2O$	$P2_1$	0.6	0.007@546	0.012@546	-	[38]
$(CN_4H_7)H_2PO_2$	$P2_12_12$	1.1	-	0.144@532	-	[39]
$(CN_4H_7)HPO_2(OH)$	$Pna2_1$	0.5	0.122@546	0.144@532	-	[39]
$(C_3H_5N_2)(H_2PO_4)$	$Pna2_1$	0.1	0.15@546	0.078@546	5.13	[40]
$(C_5H_6N)_2B_2O(HPO_4)_2$	Pc	0.7	0.156@546	0.173@546	4.41	[41]
$K[PO_2(NHCONH_2)_2]$	$Fdd2$	3.44	-	0.083@532	-	[42]
$Rb[PO_2(NHCONH_2)_2]$	$Fdd2$	2.97	-	0.088@532	-	[42]

Table S2. Crystal data and structure refinement for $[C(NH_2)]_2(PhPO_3)\cdot 2H_2O$ and $(C_5H_7N_2)_2(PhPO_3)\cdot 5H_2O$.

Empirical formula	$[C(NH_2)]_2(PhPO_3)\cdot 2H_2O$	$(C_5H_7N_2)_2(PhPO_3)\cdot 5H_2O$
Formula weight	312.28	436.40
Temperature [K]	150.15	293(2)
Crystal system	monoclinic	monoclinic
Space group (number)	*Ia* (9)	$P2_1$ (4)
a [Å]	12.4513(9)	6.67360(10)
b [Å]	7.5116(7)	17.0180(3)
c [Å]	15.8707(15)	9.8940(2)
β [°]	99.962(8)	98.031(2)
V [Å^3]	1462.0(2)	1112.65(3)
Z	4	2
ρ_{calc} [gcm^{-3}]	1.419	1.303
μ [mm^{-1}]	0.218	1.521
F(000)	664	464
Radiation	Mo K_α (λ=0.71073 Å)	Cu Kα (λ=1.54184 Å)
2θ range [°]	5.21 to 58.70	9.03 to 152.73
Index ranges	$-16 \le h \le 17$, $-10 \le k \le 10$, $-20 \le l \le 21$	$-8 \le h \le 7$, $-16 \le k \le 21$, $-12 \le l \le 12$
Reflections collected	7879	6977
Independent reflections	3176 [R_{int} = 0.0341, R_{sigma} = 0.0432]	3651 [R_{int} = 0.0258, R_{sigma} = 0.0311]
Data / Restraints / Parameters	3176 / 2 / 187	3651 / 1 / 283
Goodness-of-fit on F^2	1.077	1.054
Final R indexes [I≥2σ(I)]	R_1 = 0.0345, wR_2 = 0.0761	R_1 = 0.0281, wR_2 = 0.0686
Final R indexes [all data]	R_1 = 0.0402, wR_2 = 0.0804	R_1 = 0.0300, wR_2 = 0.0702
Largest peak/hole [eÅ^{-3}]	0.20/−0.34	0.27/−0.18
Flack X parameter	0.11(5)	0.009(13)

Table S3. Selected bond lengths for $[C(NH_2)]_2(PhPO_3)\cdot 2H_2O$ and $(C_5H_7N_2)_2(PhPO_3)\cdot 5H_2O$.

$[C(NH_2)]_2(PhPO_3)\cdot 2H_2O$

Bond	Length [Å]	Bond	Length [Å]
C1–C2	1.404(3)	C7–N3	1.319(3)
C1–C6	1.386(4)	C8–N4	1.308(4)
C2–C3	1.379(4)	C8–N5	1.314(4)
C4–C3	1.374(4)	C8–N6	1.330(4)
C4–C5	1.380(4)	P1–C1	1.811(3)
C6–C5	1.395(4)	P1–O1	1.5151(19)
C7–N1	1.319(3)	P1–O2	1.5290(19)
C7–N2	1.331(3)	P1–O3	1.5262(16)

$(C_5H_7N_2)_2(PhPO_3)\cdot 5H_2O$

Bond	Length [Å]	Bond	Length [Å]
C1–C2	1.389(4)	C14–C15	1.419(4)
C1–C6	1.385(4)	C15–C16	1.348(4)
C2–C3	1.382(4)	N1–C11	1.347(4)
C4–C3	1.362(5)	N1–C7	1.337(4)
C4–C5	1.381(6)	N2–C9	1.319(4)
C6–C5	1.387(4)	N3–C12	1.339(4)
C7–C8	1.353(4)	N3–C16	1.344(4)
C9–C8	1.410(4)	N4–C14	1.318(3)
C9–C10	1.409(3)	P1–C1	1.816(3)
C10–C11	1.345(4)	P1–O1	1.5219(17)
C13–C12	1.352(4)	P1–O2	1.5151(16)
C14–C13	1.412(3)	P1–O3	1.5251(18)

Table S4. Selected bond angles for $[C(NH_2)]_2(PhPO_3)\cdot 2H_2O$ and $(C_5H_7N_2)_2(PhPO_3)\cdot 5H_2O$.

$[C(NH_2)]_2(PhPO_3)\cdot 2H_2O$

Bond angle	Degree	Bond angle	Degree
C1–C6–C5	120.9(3)	N3–C7–N2	120.0(2)
C2–C1–P1	118.8(2)	N4–C8–N5	121.2(3)
C3–C2–C1	121.0(3)	N4–C8–N6	119.3(3)
C3–C4–C5	119.8(3)	N5–C8–N6	119.5(3)
C4–C3–C2	120.5(3)	O1–P1–C1	107.24(11)
C4–C5–C6	120.1(3)	O1–P1–O2	111.94(11)
C6–C1–C2	117.8(2)	O1–P1–O3	113.05(10)
C6–C1–P1	123.25(19)	O2–P1–C1	105.18(11)
N1–C7–N2	120.2(2)	O3–P1–C1	109.03(11)
N1–C7–N3	119.8(2)	O3–P1–O2	110.02(10)

$(C_5H_7N_2)_2(PhPO_3)\cdot 5H_2O$

Bond angle	Degree	Bond angle	Degree
C1–C6–C5	121.1(3)	C7–C8–C9	119.7(2)
C2–C1–P1	121.5(2)	C7–N1–C11	120.3(2)
C3–C2–C1	121.5(3)	N1–C7–C8	121.5(3)
C3–C4–C5	119.6(3)	N2–C9–C10	121.0(3)
C4–C3–C2	120.3(3)	N2–C9–C8	122.1(2)
C4–C5–C6	120.1(3)	N3–C12–C13	121.4(3)
C6–C1–C2	117.5(3)	N3–C16–C15	121.8(3)
C6–C1–P1	120.9(2)	N4–C14–C13	122.2(3)
C10–C11–N1	121.3(3)	N4–C14–C15	121.4(2)
C10–C9–C8	116.9(2)	O1–P1–C1	106.45(10)
C11–C10–C9	120.1(3)	O1–P1–O3	111.81(10)
C12–C13–C14	120.3(2)	O2–P1–C1	107.73(11)
C12–N3–C16	120.1(2)	O2–P1–O1	112.25(10)
C13–C14–C15	116.4(2)	O2–P1–O3	111.92(10)
C16–C15–C14	119.9(3)	O3–P1–C1	106.25(11)

Table S5. Hydrogen bonds for $[C(NH_2)]_2(PhPO_3)\cdot 2H_2O$ and $(C_5H_7N_2)_2(PhPO_3)\cdot 5H_2O$.

$[C(NH_2)]_2(PhPO_3)\cdot 2H_2O$

D–H···A [Å]	d(D–H) [Å]	d(H···A) [Å]	d(D···A) [Å]	D–H–A [°]
N2–H2A···O1#1	0.88	2.00	2.848(3)	162.2
N3–H3A···O2	0.88	1.99	2.850(3)	164.2
N4–H4A···O2	0.88	1.91	2.764(3)	163.7
N4–H4B···O5#2	0.88	2.06	2.898(4)	158.2
O4–H4C···O2	0.87	1.84	2.703(3)	172.5
O4–H4D···O3#3	0.87	1.91	2.755(3)	163.3
O5–H5C···O4	0.87	1.95	2.673(3)	140.1
O5–H5D···O1#4	0.87	1.84	2.701(3)	172.9

$(C_5H_7N_2)_2(PhPO_3)\cdot 5H_2O$

D–H···A [Å]	d(D–H) [Å]	d(H···A) [Å]	d(D···A) [Å]	D–H–A [°]
O6–H6A···O3#5	0.85	1.86	2.696(3)	167.5
O6–H6B···O1	0.85	1.88	2.706(3)	164.0
O4–H4C···O2	0.85	1.96	2.804(3)	175.6
O4–H4D···O3#6	0.85	2.06	2.862(3)	155.8
O8–H8A···O6#7	0.85	1.98	2.824(3)	172.1
O8–H8B···O7	0.85	1.97	2.815(3)	172.7
N1–H1···O1	0.86	1.86	2.710(3)	168.6
O7–H7A···O2	0.85	1.97	2.810(3)	170.6
O7–H7B···O4#8	0.85	1.99	2.821(3)	163.7
N2–H2A···O6#9	0.82	2.06	2.832(3)	156.7
N3–H3A···O3	0.86	1.84	2.685(3)	168.2
N4–H4A···O5#10	0.86	2.04	2.897(4)	171.8
N4–H4B···O2#11	0.86	2.10	2.910(3)	156.7
O5–H5A···O1	0.85	2.00	2.792(3)	154.4
O5–H5B···O8#12	0.85	2.01	2.855(4)	176.3
N2–H2B···O7#13	0.84(4)	2.14(4)	2.973(4)	171(4)

Symmetry transformations used to generate equivalent atoms:

#1: 0.5+X, -Y, +Z; #2: +X, 1.5-Y, -0.5+Z; #3: 0.5+X, 1-Y, +Z; #4: +X, 1+Y, +Z; #5: 1+X, +Y, +Z; #6: -1+X, +Y, -1+Z; #7: -1+X, +Y, +Z; #8: 2-X, 0.5+Y, 2-Z; #9: 1-X, 0.5+Y, 2-Z; #10: 1-X, 0.5+Y, 1-Z; #11: +X, +Y, 1+Z;

Table S6. FTIR spectral assignments.

FTIR (**1**)	FTIR (**2**)	
3341	3350	N–H stretching vibration, O–H stretching vibration
	3045	C–H stretching vibration
3007		C–H stretching vibration
	2937	C–H stretching vibration
	1944	out-of-plane C–H bending vibration
1650	1650	skeletal vibrations
	1533	skeletal vibrations
1434	1434	skeletal vibrations
	1205	C–N stretching vibration
1125	1127	C–N stretching vibrations
1028	1037	P–O stretching vibrations
961	959	P–O stretching vibrations
	825	C–H out-of-plane bending vibration
763	745	P–O stretching vibrations
713	710	P–O stretching vibrations
664	650	P–O stretching vibrations
577	567	O–P–O bending vibrations
523	514	O–P–O bending vibrations
499	495	O–P–O bending vibrations
457	444	O–P–O bending vibrations

Table S7. Phosphonate- and phosphate-based proton conductors reported over the past year.

Compound	Proton conductivity (S cm^{-1})	Conditions (T, RH)	Ref
PYMASH-80	5.2×10^{-2}	90 °C, 70% RH	[43]
PYMASH-90	1.37×10^{-1}	90 °C, 70% RH	[43]
PYPDSH-80	1.13×10^{-1}	90 °C, 70% RH	[43]
PYPDSH-90	3.41×10^{-1}	90 °C, 70% RH	[43]
PP-$(PhSO_3H)_2$-PAN (3:1)	3.93×10^{-2}	30 °C, 98% RH	[44]
PP-$(PhSO_3H)_2$-PAN (1:1)	1.87×10^{-2}	30 °C, 98% RH	[44]
PP-$(PhSO_3H)_2$-PAN (0.4:1)	9.17×10^{-3}	30 °C, 98% RH	[44]
PP-$(PhSO_3H)_2$-PAN (0.1:1)	5.13×10^{-3}	30 °C, 98% RH	[44]
5DPA-2Im	3.6×10^{-4}	140 °C	[45]
sPAF-225-6/QAOPBI-30	1.65×10^{-1}	200 °C	[46]
EDTMPA-PA	5.5×10^{-3}	40 °C	[47]
AOP-Me	1.62×10^{-6}	25°C, 50% RH	[48]
AOP-Et	2.65×10^{-8}	25°C, 50% RH	[48]
AOP-Ph	1.77×10^{-8}	25°C, 50% RH	[48]
AlPO	1.42×10^{-6}	25°C, 50% RH	[48]
$H_{19}Na_6[(Mo_2VO_4)_2(MoO_3)_2(\mu_2\text{-}O)_5(hedp)_3(hedpH)]\cdot 6H_2O$	2.43×10^{-6}	30°C, 50% RH	[49]
$[C(NH_2)_3]_{10}[(Mo_2VO_4)_4(\mu_2\text{-}O)_2(hpaa)_4]\cdot 6H_2O$	4.16×10^{-7}	30°C, 50% RH	[49]
$H_{11}K_4[(Co_3(AsO_4)_2(Mo_2O_2S_2)_6(OH)_6O_3(Gly)_3(H_2O)5]\cdot 35H_2O$	4.65×10^{-5}	30°C, 50% RH	[50]
$H_{16}K_4[(AsO_4)_4(Mo_2O_2S_2)_{12}(OH)_{12}O_4(H_2SDB)_6(H_2O)_2]\cdot 36H_2O$	7.83×10^{-5}	30°C, 50% RH	[50]
$H_9La(Mo_2O_4)_6(H_2O)_6(HEDP)_6\cdot 1$	2.83×10^{-4}	25°C, 98% RH	[51]

$8H_2O$			
$H_9Nd(Mo_2O_4)_6(H_2O)_6(HEDP)_6 \cdot 15H_2O$	2.34×10^{-4}	25°C, 98% RH	51
$H_9[Bi(Mo_2O_4)_6(H_2O)_6(HEDP)_6]$	2.23×10^{-4}	25°C, 98% RH	51
PP40-EDTMPA/PA	7.4×10^{-2}	160°C	52
PP50-EDTMPA/PA	8.2×10^{-2}	160°C	52
PP60-EDTMPA/PA	9.4×10^{-2}	160°C	52
PP70-EDTMPA/PA	1.2×10^{-1}	160°C	52
$H_{26}[Co_6\{N(CH_2PO_3)_2(CH_2COO)\}_6(TeMo_6O_{21})_4(H_2O)_8] \cdot 64H_2O$	2.68×10^{-5}	30°C, 55% RH	53
$H_{26}[Cu_6\{N(CH_2PO_3)_2(CH_2COO)\}_6(TeMo_6O_{21})_4(H_2O)_6] \cdot 78H_2O$	7.69×10^{-5}	30°C, 55% RH	53
$H_{34}Na_2[Co_8\{N_2(CH_2)_2(CH_2PO_3)_3(CH_2PO_3H_2)\}_4(TeMo_6O_{21})_6(PO_3)_4(H_2O)_{16}] \cdot 84H_2O$	5.48×10^{-5}	30°C, 55% RH	53
$Ce[(H_3L)(C_2O_4)0.5(H_2O)] \cdot 0.5H_2O$	1.22×10^{-3}	95 °C, 95% RH	54
$Ce[(H_4L)(H_3L)(H_2O)] \cdot 2H_2O$	6.51×10^{-4}	95 °C, 95% RH	54
$[Co(H_2O)4(4,4'bpy)2][H_3L1]_2 \cdot 10H2O$	8.4×10^{-5}	50°C, 95% RH	55
PFPYSH-60	3.37×10^{-2}	30 °C	56
PFPYSH-70	5.33×10^{-2}	30 °C	56
PFPYSH-80	7.64×10^{-2}	30 °C	56
PFPYSH-90	1.15×10^{-1}	30 °C	56
$[Cd_2(L1)_2(Bib)_2(H_2O)] \cdot 4.5H_2O$	3.51×10^{-5}	95°C, 95% RH	57
$[Cd(L2)(Bib)] \cdot 3H_2O$	1.21×10^{-5}	95°C, 95% RH	57

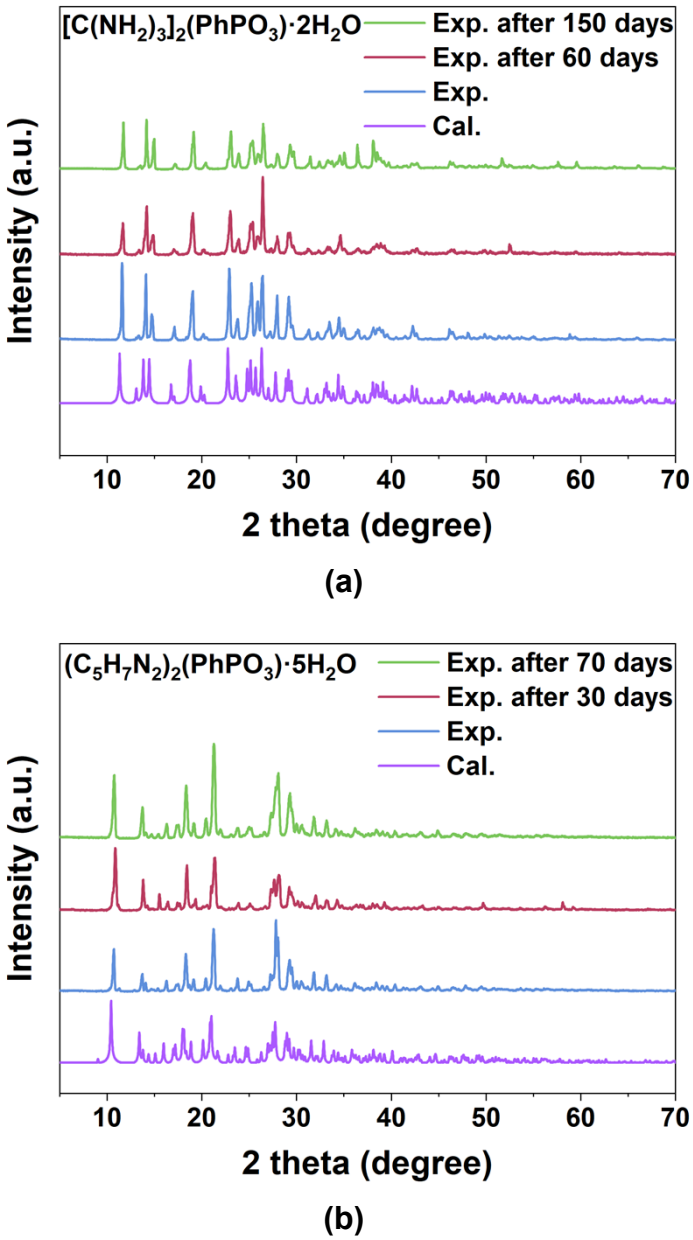

Figure S1. Experimental and calculated PXRD patterns for $[C(NH_2)]_2(PhPO_3)\cdot 2H_2O$ (a) and $(C_5H_7N_2)_2(PhPO_3)\cdot 5H_2O$ (b) after air exposure.

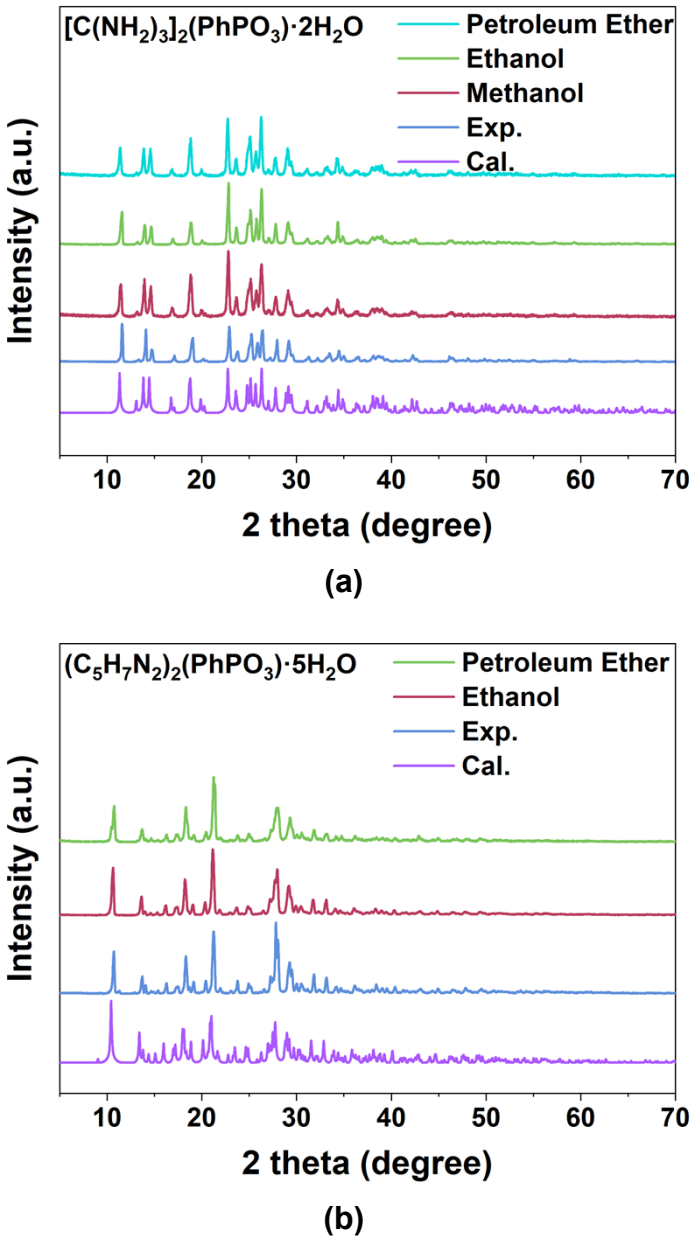

Figure S2. Experimental and calculated PXRD patterns for $[C(NH_2)]_2(PhPO_3)\cdot 2H_2O$ (a) and $(C_5H_7N_2)_2(PhPO_3)\cdot 5H_2O$ (b) after soaking in various organic solvents for 72 hours.

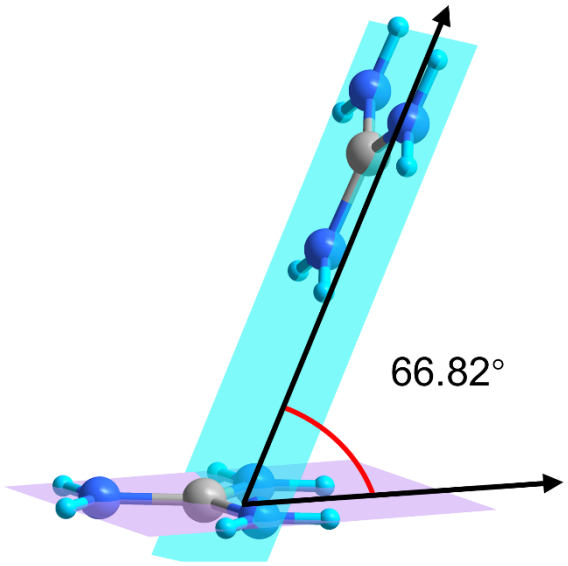

Figure S3. Angle between the planar conjugated groups in the asymmetric unit of $[C(NH_2)]_2(PhPO_3)\cdot 2H_2O$.

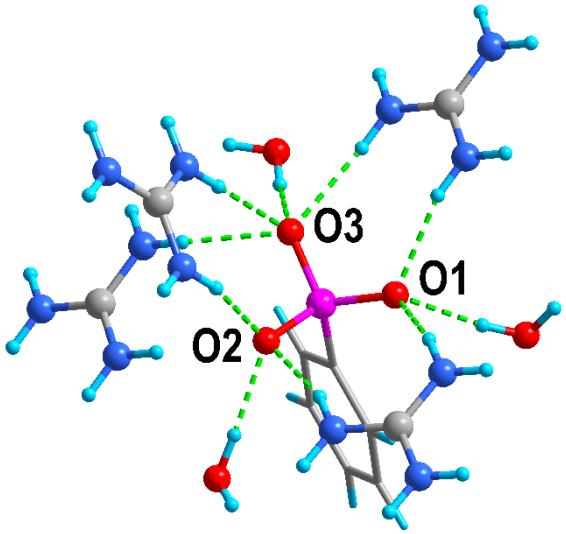

Figure S4. Hydrogen-bonding interactions of the $(PhPO_3)^{2-}$ anions with surrounding planar π-conjugated cations and water molecules in $[C(NH_2)]_2(PhPO_3)\cdot 2H_2O$.

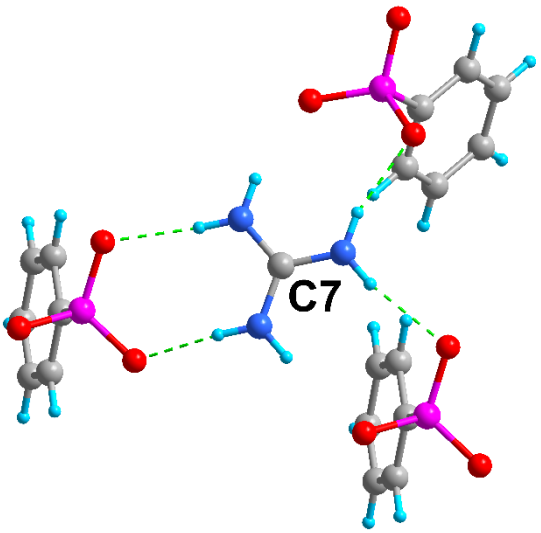

(a)

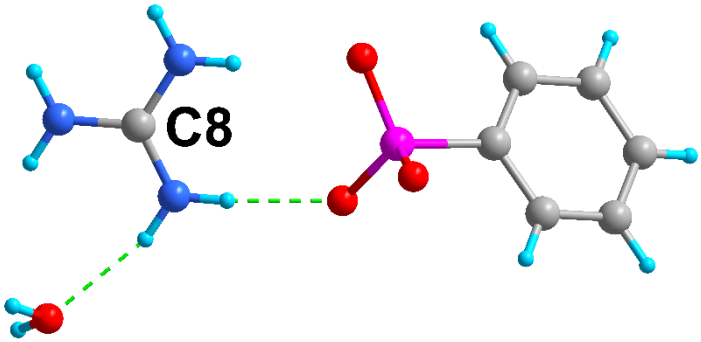

(b)

Figure S5. Hydrogen-bonding interactions of the $[C(NH_2)_3]^+$ cations with surrounding $(PhPO_3)^{2-}$ anions and water molecules in $[C(NH_2)]_2(PhPO_3)\cdot 2H_2O$.

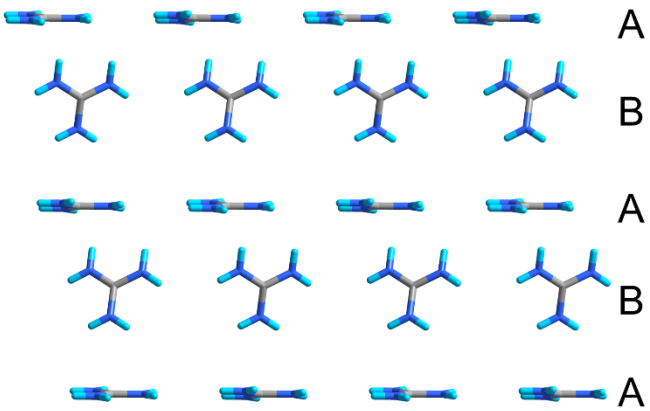

Figure S6. Arrangement of the $[C(NH_2)_3]^+$ units in $[C(NH_2)]_2(PhPO_3)\cdot 2H_2O$.

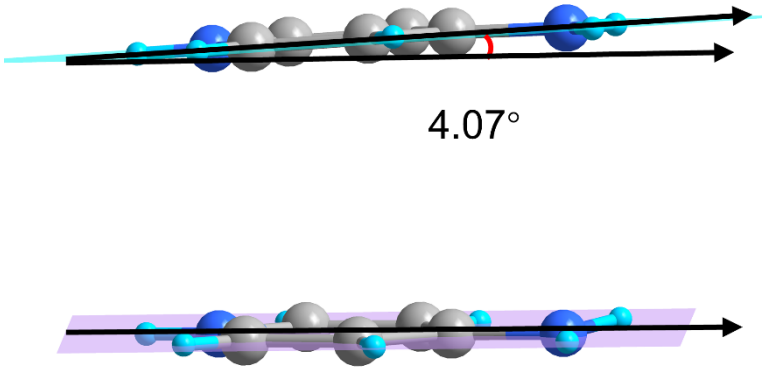

Figure S7. Angle between the 4-aminopyridinium cations in the asymmetric unit of $(C_5H_7N_2)_2(PhPO_3)\cdot 5H_2O$.

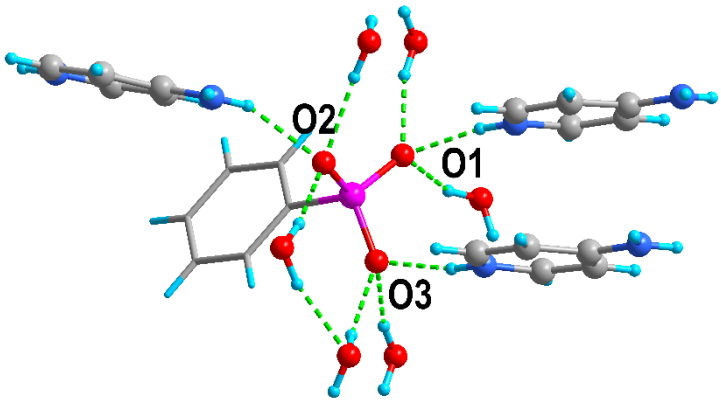

Figure S8. Hydrogen-bonding interactions of the $(PhPO_3)^{2-}$ anions with surrounding planar π-conjugated cations and water molecules in $(C_5H_7N_2)_2(PhPO_3)\cdot 5H_2O$.

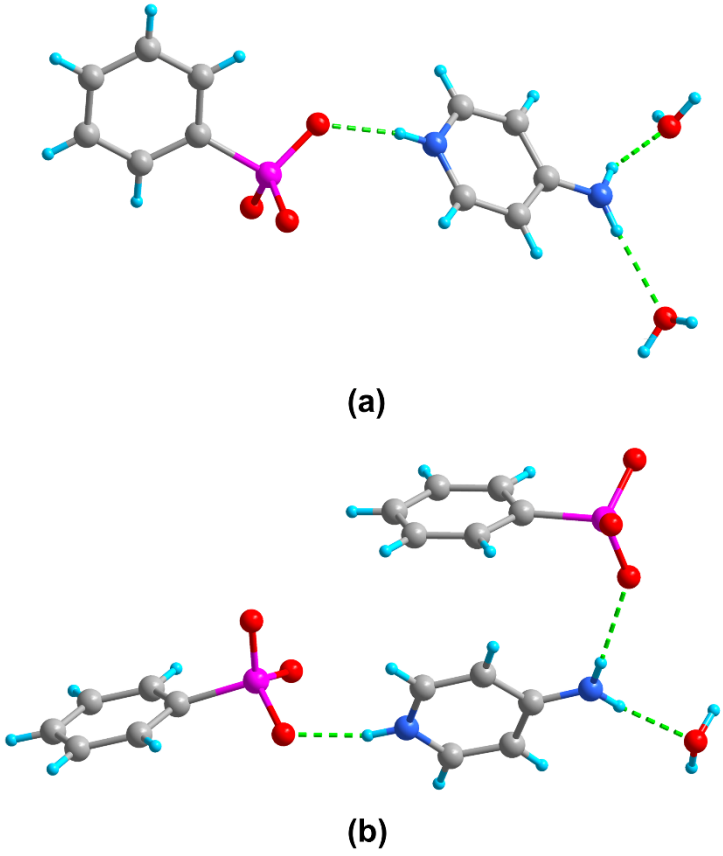

Figure S9. Hydrogen-bonding interactions of the $(C_5H_7N_2)^+$ cations with surrounding $(PhPO_3)^{2-}$ anions and water molecules in $(C_5H_7N_2)_2(PhPO_3)\cdot 5H_2O$.

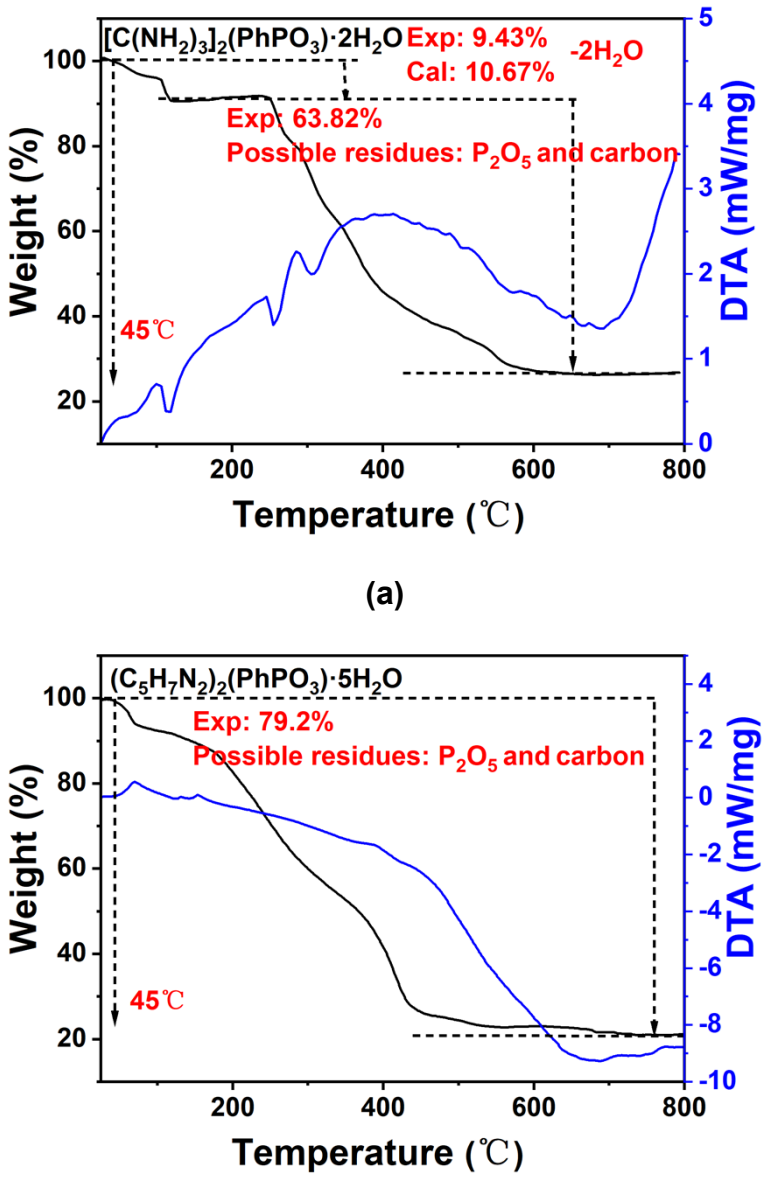

Figure S10. TGA and DTA curves of $[C(NH_2)]_2(PhPO_3)\cdot 2H_2O$ (a) and $(C_5H_7N_2)_2(PhPO_3)\cdot 5H_2O$ (b) under N_2 atmosphere.

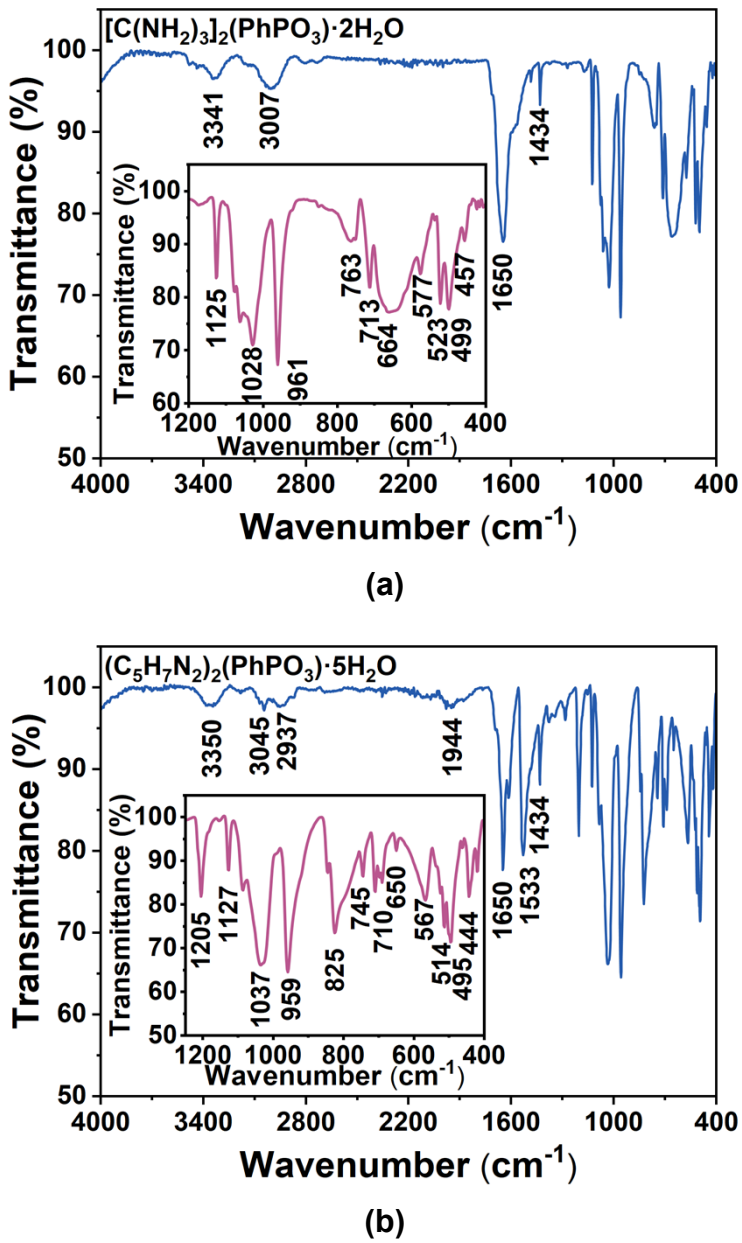

Figure S11. Infrared spectra of $[C(NH_2)]_2(PhPO_3)\cdot 2H_2O$ (a) and $(C_5H_7N_2)_2(PhPO_3)\cdot 5H_2O$ (b).

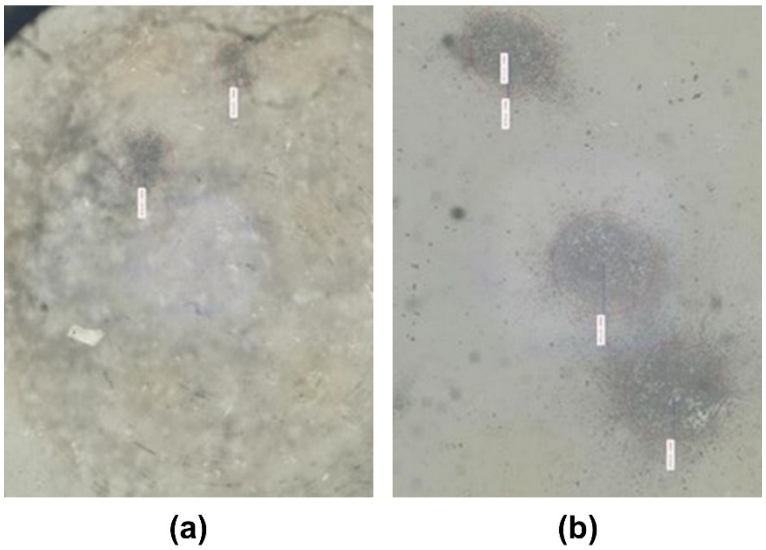

Figure S12. Optical micrographs of the laser-damaged areas on compressed samples of $[C(NH_2)]_2(PhPO_3)\cdot 2H_2O$ (a) and $(C_5H_7N_2)_2(PhPO_3)\cdot 5H_2O$ (b).

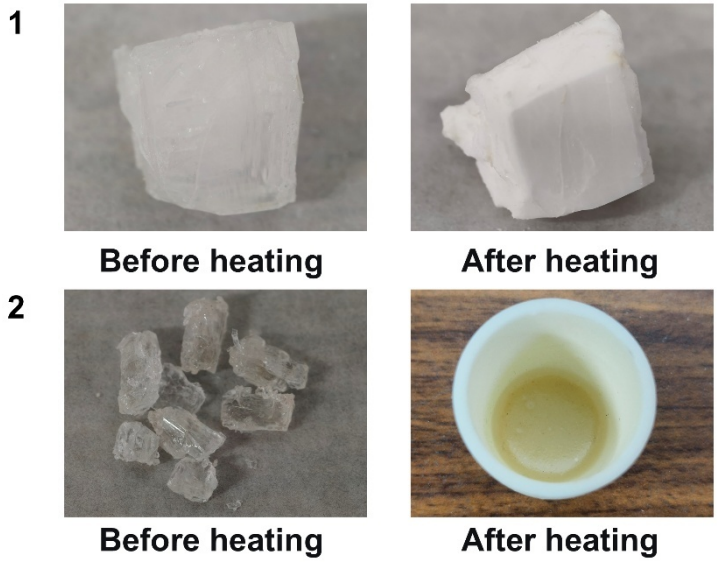

Figure S13. Photographs of the crystals of compounds **1** and **2** after being heated in air at 150 °C for one hour and then naturally cooled to room temperature (RT).

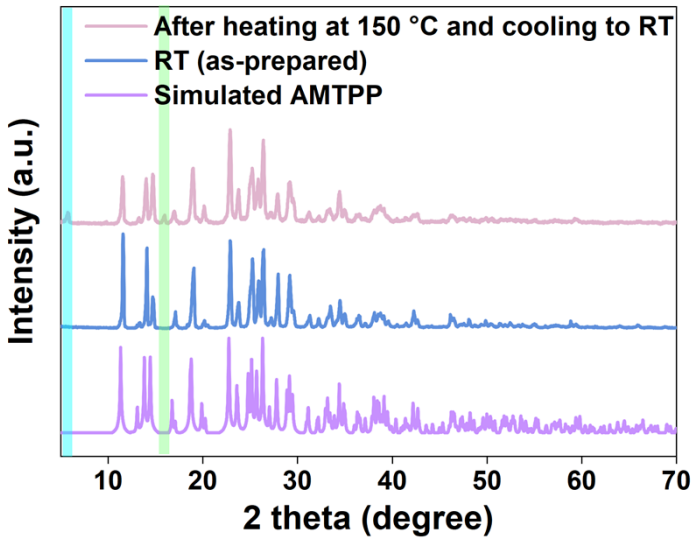

Figure S14. Simulated and experimental XRD patterns of $[C(NH_2)]_2(PhPO_3)\cdot 2H_2O$ (**1**) at room temperature and after treatment at 150 °C (cooled to RT).

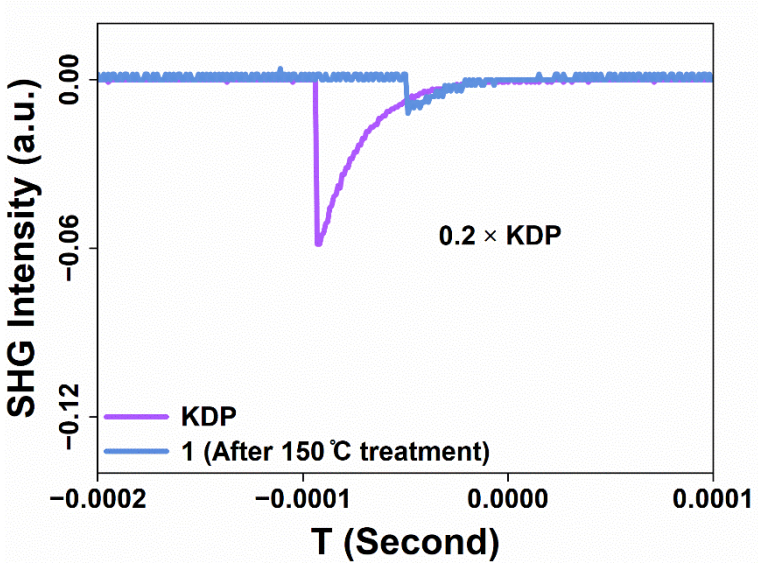

Figure S15. SHG signals of $[C(NH_2)]_2(PhPO_3)\cdot 2H_2O$ (**1**) (after treatment at 150 °C) and KDP under 1064 nm laser irradiation. Particle size: 150–210 μm.

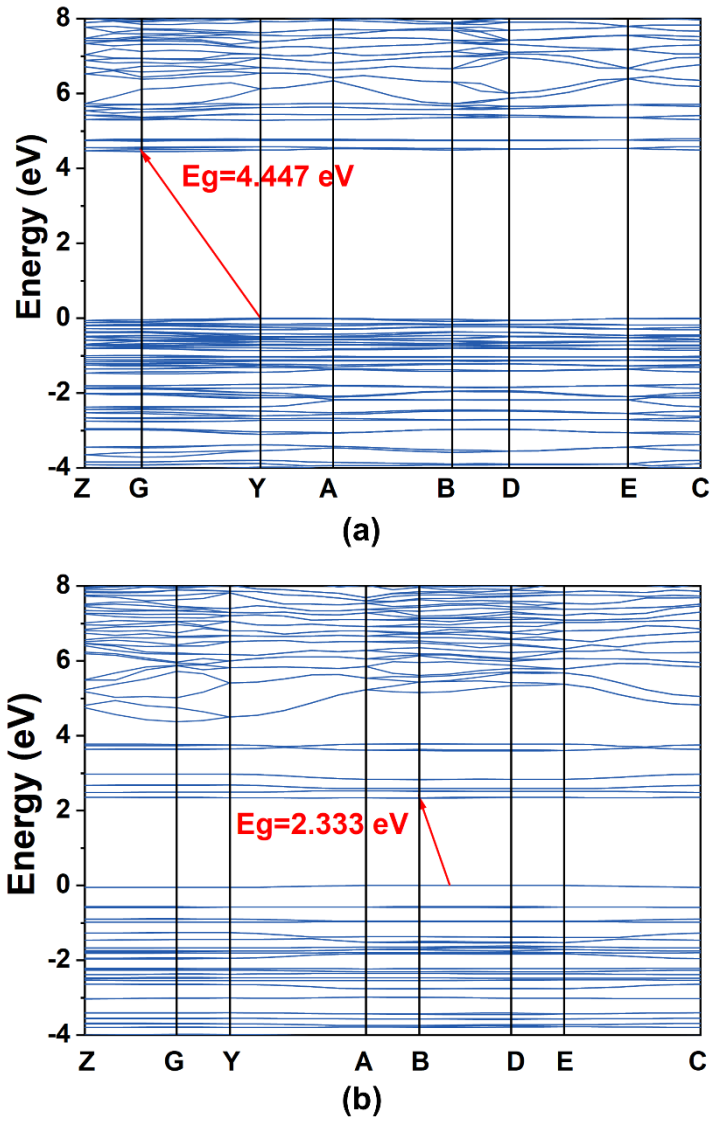

Figure S16. Calculated band gap of $[C(NH_2)]_2(PhPO_3)\cdot 2H_2O$ (a) and $(C_5H_7N_2)_2(PhPO_3)\cdot 5H_2O$

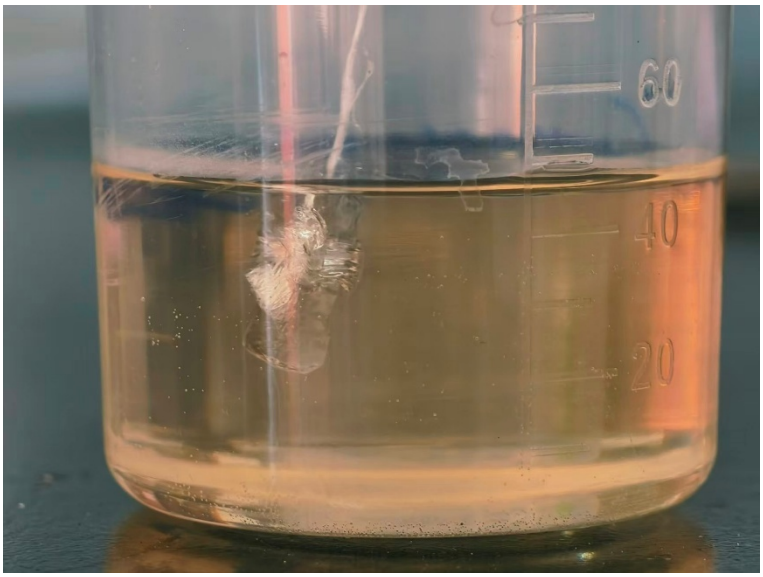

Figure S17. Single-crystal growth via the seed crystal method.

References

1 R. H. Blessing, An empirical correction for absorption anisotropy, *Acta Crystallogr. A*, 1995, **51**, 33–38.

2 G. M. Sheldrick, *SHELXT* – integrated space-group and crystal-structure determination, *Acta Crystallogr. Sect. Found. Adv.*, 2015, **71**, 3–8.

3 G. M. Sheldrick, Crystal structure refinement with *SHELXL*, *Acta Crystallogr. Sect. C Struct. Chem.*, 2015, **71**, 3–8.

4 A. L. Spek, Single-crystal structure validation with the program *PLATON*, *J. Appl. Crystallogr.*, 2003, **36**, 7–13.

5 H. D. Flack, On enantiomorph-polarity estimation, *Acta Crystallogr. A*, 1983, **39**, 876–881.

6 P. Kubelka and F. Munk, An article on optics of paint layers, *Z. Phys.*, 1931, **2**, 593–609.

7 S. K. Kurtz and T. T. Perry, A powder technique for the evaluation of nonlinear optical materials, *J. Appl. Phys.*, 1968, **39**, 3798–3813.

8 V. Milman, B. Winkler, J. A. White, C. J. Pickard, M. C. Payne, E. V. Akhmatskaya and R. H. Nobes, Electronic structure, properties, and phase stability of inorganic crystals: A pseudopotential plane-wave study, *Int. J. Quantum Chem.*, 2000, **77**, 895–910.

9 M. D. Segall, P. J. D. Lindan, M. J. Probert, C. J. Pickard, P. J. Hasnip, S. J. Clark and M. C. Payne, First-principles simulation: ideas, illustrations and the CASTEP code, *J. Phys. Condens. Matter*, 2002, **14**, 2717–2744.

10 J. P. Perdew, K. Burke and M. Ernzerhof, Generalized gradient approximation made simple, *Phys. Rev. Lett.*, 1996, **77**, 3865–3868.

11 J. S. Lin, A. Qteish, M. C. Payne and V. Heine, Optimized and transferable nonlocal separable *ab initio* pseudopotentials, *Phys. Rev. B*, 1993, **47**, 4174–4180.

12 S. Sharma, J. K. Dewhurst and C. Ambrosch-Draxl, Linear and Second-order Optical Response of the III-V Mono-layer Superlattices, *Phys. Rev. B*, 2003, **67**, 165332.

13 J. E. Sipe and E. Ghahramani, Nonlinear optical response of semiconductors in the independent-particle approximation, *Phys. Rev. B*, 1993, **48**, 11705–11722.

14 P. Tang, X. Wen, J. Chen, N. Ye and G. Peng, $Ag(Te_2O_3)(PO_4)$: The first Ag-containing phosphate-tellurite nonlinear optical crystal featuring novel zigzag layered structure, *Chin. J. Struct. Chem.*, 2026, **45**, 100763.

15 H. Jiang, J. Zhao, C. Li, S. Yang, D. Cai, H. Jiang, X. Duan and F. Yu, Growth, structure and optical properties of $PbBi_3PO_8$ crystals, *J. Solid State Chem.*, 2026, **353**, 125672.

16 Y. Pan, J. Deng, Y. Hao, X. Zhao, Y. Bao, Z. Fang, C. Deng, K. Hu, W. Cheng and Y. Lin, Syntheses, structural characterization, and nonlinear optical properties of mixed alkaline/alkaline earth metal borophosphates, *J. Solid State Chem.*, 2025, **352**, 125575.

17 H. J. Huang, X. H. Kong, H. J. Zhao, N. Ye, Z. G. Hu and C. G. Li, A-site cation substitution toward structural transformation in phosphates exhibiting short UV transparency and second harmonic response, *Inorg. Chem.*, 2025, **64**, 17083–17090.

18 Y. Hao, C. Chen, C. Hou, X. Zhao, Y. Lin, R. Zhang, H. Lu, K. Hu, W. Cheng and M. Liang, Design, Synthesis, and Improvement of Nonlinear Optical Properties from Aluminophosphite to Aluminophosphate, *Inorg. Chem.*, 2025, **64**, 13805–13814.

19 X. Zhang, J. Q. Shen, H. X. Lv, P. H. Guo, Y. G. Chen, C. L. Hu and X. M. Zhang, Deep-ultraviolet nonlinear-optical crystals $LiBePO_4$ and BeP_2O_6 synthesized by ionic potential modulation towards uniform arrangement of PO_4 groups, *Inorg. Chem. Front.*, 2025, **12**, 5430–5438.

20 S. Chen, Z. Bai, X. Song, T. Ouyang, Y. Li, Q. Ding, H. Wang, W. Chen, J. Luo and S. Zhao, A HTO-Type Nonlinear Optical Fluorophosphate with Ultrawide Bandgap, *Small*, 2025, **21**, 2408191.

21 H. Zhao, C. Li, J. Lu, Z. Yang, J. Han and S. Pan, Deep ultraviolet transparent borophosphates $LiAB_2P_2O_9$ (A = NH_4 , K) and $LiNaB_2P_2O_8(OH)_2{\cdot}H_2O$ exhibiting a moderate second-harmonic generation response, *J. Mater. Chem. C*, 2025, **13**, 3251–3258.

22 Y. Hao, C. Chen, C. Hou, S. Liu, Z. Peng, Y. Lin, H. Li, X. Zhao, K. Koirala, H. Lu, C. Deng and K. Hu, $Li_3[AlP_2O_7F(OH)](H_2O)_{0.5}$ and $A[Al_2(PO_4)_2F(H_2O)](A = K, Rb)$: Counter Cation Templates Derived Three Polar Alkaline Metal Fluoroaluminophosphates, *Inorg. Chem.*, 2024, **63**, 24885–24895.
23 X. Bai, X. Su and W. Jin, $MgPO_2F_3$: An Ultraviolet Nonlinear Optical System with an Extremely Short Phase-Matching Wavelength Achieved by Introducing Dual-Type Fluorine via Structure Prediction, *J. Phys. Chem. C*, 2024, **128**, 21173–21181.
24 J. Zhang, Q. Yue, S. Zhou, X. Wu, H. Lin and Q. Zhu, Screening Strategy Identifies an Overlooked Deep-Ultraviolet Transparent Nonlinear Optical Crystal, *Angew. Chem. Int. Ed.*, 2024, **63**, e202413276.
25 R. L. Tang, L. Ma, Y. L. Lv, W. Liu and S. P. Guo, From $Pb_6(HPO_3)(H_2PO_3)Cl_9$ to $Pb_6(HPO_3)_2Br_8(H_2O)\cdot H_2O$: Halogen Regulation to Achieve Inorganic Metal Phosphite Halide Nonlinear Optical Material with Unprecedented Pb-Centered Polyhedral Units, *Inorg. Chem.*, 2024, **63**, 13197–13201.
26 Y. Tian, W. Zeng, X. Dong, L. Huang, Y. Zhou, H. Zeng, Z. Lin and G. Zou, Enhanced UV Nonlinear Optical Properties in Layered Germanous Phosphites through Functional Group Sequential Construction, *Angew. Chem. Int. Ed.*, 2024, **63**, e202409093.
27 L. Ma, Y. L. Lv, X. F. Ao, W. Liu, S. P. Guo and R. L. Tang, Centric $Sc(HPO_3)(H_2PO_3)(H_2O)$ and Acentric $Sc(H_2PO_3)_3$: Two Ultraviolet Scandium Phosphite Optical Crystals, *Inorg. Chem.*, 2024, **63**, 7118–7122.
28 L. Wu, H. Tian, C. Lin, X. Zhao, H. Fan, P. Dong, S. Yang, N. Ye and M. Luo, Optimized arrangement of non-π-conjugated PO_3NH_3 units leads to enhanced ultraviolet optical nonlinearity in $NaPO_3NH_3$, *Inorg. Chem. Front.*, 2024, **11**, 1145–1152.
29 Q. Jing, M. Zhu, L. Li, X. Ji, H. Duan, H. Chen and M. H. Lee, Two noncentrosymmetric alkali metal phosphates $MZnPO_4$ (M = Rb, Cs) with honeycomb-like structures, *Opt. Mater.*, 2024, **147**, 114620.
30 X. Pan, F. Liu, Z. Lin and L. Kang, Birefringent Dispersion Optimization to Achieve Superior Nonlinear Optical Phase Matching in Deeper Solar-Blind UV Band from KH_2PO_4 to BeH_3PO_5, *Small*, 2024, **20**, 2308811.
31 L. Wu, R. Zhang, Q. Jing, H. Huang, X. He, Z. Wang and Z. Chen, Modulating optical performance by phase transition in a nonlinear optical material β-$Li_2RbBi(PO_4)_2$, *Inorg. Chem. Front.*, 2023, **10**, 4496–4502.
32 Y. L. Sun, G. X. Liu, Y. L. Lv, L. Ma, W. D. Yao and R. L. Tang, $(NH_4)_3(H_3O)Zn_4(PO_4)_4$: A nonlinear optical zinc orthophosphate crystal, *J. Solid State Chem.*, 2023, **325**, 124171.
33 H. Liu, H. Wu, Z. Hu, J. Wang, Y. Wu and H. Yu, $Cs_3[(BOP)_2(B_3O_7)_3]$: A Deep-Ultraviolet Nonlinear Optical Crystal Designed by Optimizing Matching of Cation and Anion Groups, *J. Am. Chem. Soc.*, 2023, **145**, 12691–12700.
34 X. He, L. Qi, W. Zhang, R. Zhang, X. Dong, J. Ma, M. Abudoureheman, Q. Jing and Z. Chen, Controlling the Nonlinear Optical Behavior and Structural Transformation with A-Site Cation in α-$AZnPO_4$ (A = Li, K), *Small*, 2023, **19**, 2206991.
35 W. Liu, M. H. Lee, R. Guo and J. Yao, Structure and Characterization of $K_2Na_3B_2P_3O_{13}$, a New Nonlinear Optical Borophosphate with One-Dimensional Chain Structure and Short Ultraviolet Cutoff Edge, *Inorg. Chem.*, 2023, **62**, 2480–2488.
36 G. Xu, X. Bai, Z. Yang, J. Han and S. Pan, π-Conjugated Cations in Phosphates: A Pathway to Solar-Blind UV Nonlinear Optical Crystals with Phase-Matching, *Angew. Chem. Int. Ed.*, 2025, **64**, e202510363.
37 S. Li, Y. Zhu, Z. Geng, R. Fu, J. Zeng, Y. Luo, S. Lei and Z. J. Ma, An excellent ultraviolet nonlinear optical crystal derived from the polar methylphosphonate unit, *Mater. Chem. Front.*, 2025, **9**, 1375–1382.

38 K. Huang, X. M. Dong, C. He, Z. X. Zhao, W. Chen, H. Y. Zhao, J. X. Hu, Q. Wei and G.-M. Wang, Chiral-unit-oriented design of non-π-conjugated noncentrosymmetric phosphates with short absorption edges, *J. Phys. Chem. Lett.*, 2025, **16**, 1881–1886.
39 W. B. Zhang, M. Arif, H. Zhou, R. An, Z. H. Yang, X. L. Hou, S. L. Pan and S. J. Han, Highly polarizable phosphorus-centered tetrahedra and π-conjugated carbon-centered triangular moieties inducing large anisotropy and short-wavelength phase-matching, *Adv. Opt. Mater.*, 2025, **13**, 2403372.
40 Q. Xia, X. Jiang, L. Qi, C. Wu, Z. Lin, Z. Huang, M. G. Humphrey, K. Tatsumi and C. Zhang, Large optical anisotropy in noncentrosymmetric phosphate with pseudo 2D intercalated layer, *Inorg. Chem. Front.*, 2024, **11**, 8813–8823.
41 H. Zhang, D. Jiao, X. Li, C. He, X. Dong, K. Huang, J. Li, X. An, Q. Wei and G. Wang, A Noncentrosymmetric Metal-Free Borophosphate: Achieving a Large Birefringence and Excellent Stability by Covalent-Linkage, *Small*, 2024, **20**, 2401464.
42 F. Chen, F. Mo, H. Chen, M. J. Lin and Y. Chen, $KPO_2(NHCONH_2)_2$: A Promising Deep-Ultraviolet Nonlinear Optical Phosphate Containing Polar $[PO_2(NHCONH_2)_2]^-$ Tetrahedra, *Chem. Mater.*, 2024, **36**, 2985–2992.
43 B. Ghanti, B. Voit and S. Banerjee, Superprotonic membranes from phosphonic acid-anchored pyridinyl sulfonated polytriazoles: toward intrinsic PA doping, *ACS Appl. Polym. Mater.*, 2025, **7**, 15004–15018.
44 J. Afzal, J. Zhang and H. Wang, Fabrication of $–SO_3$ H-functionalized polyphosphazene-reinforced proton conductive matrix-mixed membranes, *RSC Adv.*, 2024, **14**, 14456–14464.
45 Y. Shigeta, M. Annen, N. Hosoe, T. Kurihara, S. Amemori, T. Ida and M. Mizuno, Annealing-induced local structure and molecular dynamics effects enhance the proton conductivity of a bisimidazolium diphosphonate salt, *J. Phys. Chem. C*, 2026, **130**, 4945–4955.
46 K. Xu, H. Mi, X. Zong, Y. Xie, Z. Sun, B. Liu, X. Liu and W. Hu, sPAF-225/QAOPBI composite high-temperature proton exchange membrane with robust acid-base interaction and controlled phosphoric acid, *Eur. Polym. J.*, 2026, **244**, 114518.
47 X. Wang, J. Yao, Z. Zhang, J. Zhang, B. Liu, W. Liu, W. Li, S. Lu, Y. Xiang, H. Wang, S. P. Jiang and J. Zhang, Machine learning-guided gradient dual-proton conducting catalytic layers for high temperature proton exchange membrane fuel cells in aviation, *Engineering*, 2025, S2095809925006721.
48 T. Ami, K. Oka, H. Kasai and T. Kimura, Proton conductivity at the controlled hydrophilic and hydrophobic surfaces of mesoporous aluminum organophosphonates, *J. Mater. Chem. A*, 2026, **14**, 3863–3873.
49 Q. Liu, S. Liu, Y. Cui, Y. Chen, S. Liang and H. Y. Zang, Organic-ligand functionalization of $[MoV_2O_4]^{2+}$ clusters: assembly, characterization, and enhanced proton conduction, *J. Mol. Struct.*, 2026, **1350**, 144037.
50 L. Wang, J. Li, X. Liu, Q. Liu, J. Li, S. Liang and H. Y. Zang, Ligand-directed assembly of $[Mo_2O_2S_2]^{2+}$ into interlocked architectures with efficient proton conduction, *Chin. Chem. Lett.*, 2025, 111698.
51 J. Li, L. Wang, Q. Liu, S. Yu, H. Y. Zang and Z. M. Su, Ln^{3+}/Bi^{3+}-induced the assembly of molybdenum-oxygen clusters with proton conductivity, *Chin. Chem. Lett.*, 2025, 111532.
52 W. Li, J. Fang, Z. Mao, S. Lu and Y. Xiang, Dispersion engineering of ethylenediamine tetramethylene phosphonic acid in composite membranes: toward enhanced proton conductivity and phosphoric acid retention for high-temperature proton exchange membranes, *J. Membr. Sci.*, 2025, **734**, 124388.
53 Q. Liu, J. Ma, L. Xiao, S. Liu, Y. Chen, L. Wang, Y. Cui, S. Liang and H. Y. Zang, Controlled assembly of phosphonic acid ligand covalently modified $[TeMo_6O_{21}]^{2-}$ polyanions for proton conduction, *Chin. Chem. Lett.*, 2025, 111413.

54 X. Li, J. H. Yu, L. Y. Sun, Y. F. Xing, X. Zhang, C. Q. Jiao, H. W. Zheng, Y. Y. Zhu and Z. G. Sun, Two stable proton–conductive cerium (III)–organic frameworks with high–density carboxylic groups, *J. Solid State Chem.*, 2025, **348**, 125367.
55 S. M. Elahi, Phosphonocarboxylates in mixed-ligated approach with diverse structural features (0D to 3D), and studies of non-covalent interactions for revealed proton conduction, *Chem. – Asian J.*, 2025, **20**, e202401887.
56 B. Ghanti, R. Kamble, H. Komber, B. Voit and S. Banerjee, High proton-conducting phosphine oxide- and pyridinyl-based fluoro-sulfonated proton exchange membranes with enhanced chemical stability, *J. Power Sources*, 2025, **631**, 236201.
57 Y. N. Zhou, D. Y. Liu, J. H. Yu, X. Li, C. Y. Huang, H. W. Zheng, C. Q. Jiao, Y. Y. Zhu and Z. G. Sun, Two dual–functional cadmium phosphonate materials: fluorescent sensing of benzophenone and proton conduction, *J. Mol. Struct.*, 2025, **1329**, 141418.